SECOND EUROPEAN CONFERENCE ON EARTHQUAKE ENGINEERING
AND SEISMOLOGY, ISTANBUL AUG. 25-29, 2014

EFFECTS OF GROUND MOTION INPUT ON THE DERIVED FRAGILITY FUNCTIONS

Ufuk HANCILAR[1], Ebru HARMANDAR[2] and Eser ÇAKTI[3]

ABSTRACT

Empirical fragility functions are derived by statistical processing of the data on: i) Damaged and undamaged buildings, and ii) Ground motion intensity values at the buildings' locations. This study investigates effects of different ground motion inputs on the derived fragility functions. The previously constructed fragility curves (Hancilar et al., 2013), which rely on specific shaking intensity maps published by the USGS after the 2010 Haiti Earthquake, are compared with the fragility functions computed in the present study. Building data come from field surveys of 6,347 buildings that are classified with respect to structural material type and number of stories. For damage assessment, the European Macroseismic Scale (EMS-98) damage grades are adopted.

The simplest way to account for the variability in ground motion input could have been achieved by employing different ground motion prediction equations (GMPEs) and their standard variations. However, in this work, we prefer to rely on stochastically simulated ground motions of the Haiti earthquake. We employ five different source models available in the literature and calculate the resulting strong ground motion in time domain. In our simulations we also consider the local site effects by published studies on NEHRP site classes and micro-zoning maps of the city of Port-au-Prince. We estimate the regional distributions from the waveforms simulated at the same coordinates that we have damage information from. The estimated spatial distributions of peak ground accelerations, PGAs, are then used as input to fragility computations.

INTRODUCTION

Empirical methods employ damage data from historical earthquakes for the development of fragility functions. The observed damage at various locations is correlated to a ground motion intensity measure such as peak ground acceleration (PGA) or macroseismic intensity and, as a result of this statistical process fragility functions are generated (Spence et al., 1992). By the use of real observational data, all the characteristics of strong ground shaking, i.e. source and path information and local soil conditions, as well as the variations in the exposed buildings' performances under earthquake loadings are inherently taken into account. Such a data set should consist of a sufficient number of observations relying on consistent and representative building survey information for both damaged and undamaged buildings (Sarabandi et al., 2004). This can be achieved by using standardized survey forms, adopting pre-defined structural system descriptions and performing damage assessments on the basis of a common damage categorization scheme for the identified structural system types. The construction of empirical fragility functions also requires the

[1] Assoc. Prof. Dr., Department of Earthquake Engineering, Boğaziçi University, Istanbul, hancilar@boun.edu.tr
[2] Dr., Department of Earthquake Engineering, Boğaziçi University, Istanbul, ebru.harmandar@boun.edu.tr
[3] Prof. Dr., Department of Earthquake Engineering, Boğaziçi University, Istanbul, eser.cakti@boun.edu.tr

characterisation of the corresponding ground motion intensity levels that the buildings in the sample were experienced. Ideally, real ground motion recordings across the surveyed areas would be used for intensity level assignments. However, due to the scarcity of ground motion recordings, ground motion intensity values, in practice, are obtained through ground motion prediction equations (GMPEs). The selected GMPE should be representative of the earthquake event and the site in terms of faulting mechanisms and soil types. This implies that changing the GMPE would result in different ground motion intensity level estimations.

If one of the two inputs in the derivation of empirical fragility functions, i.e. inventory of damaged and undamaged buildings and ground motion intensity values at each of the surveyed buildings, is changed the resulting fragility functions might be different. Rota et al. (2008) conducted a sensitivity analysis to see the effect of randomly varying the PGA at their sites by up to 50%. They observe little differences in the resulting mean fragility curves, up to 10% in the exceedance probabilities of the larger damage states. Rossetto et al. (2013) reports that since Rota et al (2008) use bins of PGA values for regression, this binning process may result in less observed variability than if a direct regression were carried out. Colombi et al. (2008) consider two different GMPEs in the derivation of spectral displacement based empirical fragility functions. They find that the epistemic uncertainty in the GMPE has a large influence on the fragility curves generated, as they predict widely different spectral displacement values for the same building classes. Another argument is if the ground motion input is changed while the size of damage data is adequately large, how much difference in the resulting fragility functions, especially in their shapes, would be observed since they are obtained by means of statistical inference techniques.

This study aims to investigate the influence of altering ground motion input on the resulting fragility curves. For the derivation of fragility functions, the same data set of the damaged buildings collected after the 2010 Haiti earthquake and the same methodology as provided in Hancilar et al. (2013) are used. Empirical fragility functions are constructed for five different ground motion inputs that are obtained by stochastic ground motion simulations. The produced fragilities are compared with the previously constructed fragility curves by Hancilar et al. (2013), which rely on specific shaking intensity maps published by the USGS after the 2010 Haiti Earthquake.

DESCRIPTION OF DAMAGE DATA

In the immediate aftermath of the Haiti earthquake of 12 January 2010, there was an unprecedented international effort undertaken by scientists and engineers from all over the world to exploit the newly released remote sensing data for mapping damage and for aiding the recovery efforts (Corbane et al., 2011). A joint work for the estimation of damages to the building stock based on aerial images was carried out by the United Nations Institute for Training and Research (UNITAR) Operational Satellite Applications Programme (UNOSAT), the European Commission (EC) Joint Research Centre (JRC) and the World Bank/ImageCAT in support of the Post Disaster Needs Assessment and Recovery Framework (PDNA). A targeted field campaign was also led to the areas affected by the disaster in collaboration with the Centre National d'Information Géo-Spatial (CNIGS) representing the Government of Haiti, with the purpose of validating the remote sensing based damage assessment. These two methodologies for collecting data resulted in two data sets of the damaged buildings categorised according to European Macroseismic Scale (EMS-98) (Grünthal, 1998) damage grades, i.e. DG-1, DG-2, DG-3, DG-4 and DG-5. In this study, fragility functions are derived only for the data set coming from field surveys.

In total, 6,900 buildings were surveyed in the field. After the quality checks, 6,492 buildings were retained in the data set. The sample was sorted with respect to three attribute fields: damage grades, number of storeys and construction material/structural type. Concerning the number of storeys, the buildings were divided into two groups: 1-2 storey buildings and 3-5 storey buildings, which can be considered as low- and mid-rise buildings, respectively. With regards to structural system, reinforced concrete (RC) frames and wooden frames were identified. There were also some buildings made of steel frames, but they did not taken into account in the fragility analyses. According to this classification a breakdown of the number of buildings assessed at each damage state is given in Table 1.

Table 1. Field data set: Number of assessed buildings by structural material type, number of storeys and damage grade. Numbers in parenthesis present percentages of the buildings at that damage state.

	EMS-98 Damage Grades						
	No damage	**DG-1**	**DG-2**	**DG-3**	**DG-4**	**DG-5**	**Total**
				RC Frame			
1-2 storey	1,956 (38%)	1,198 (23%)	645 (13%)	496 (10%)	356 (7%)	475 (9%)	5,126
3-5 storey	97 (28%)	44 (13%)	40 (12%)	39 (11%)	37 (11%)	88 (25%)	345
				Wooden Frame			
1-2 storey	367 (42%)	163 (19%)	101 (12%)	87 (10%)	78 (9%)	80 (9%)	876
							6,347

GROUND MOTION SIMULATION

We use a stochastic finite-fault technique based on a dynamic corner frequency for ground motion simulation. Fault is divided into N sub-faults, where each sub-fault is considered as a small point source in finite-fault modeling of earthquake ground motions. The ground motions contributed by each sub-fault can be calculated by the stochastic point-source method and then summed at the observation point, with an appropriate time delay, to obtain the ground motion from the entire fault. The acceleration spectrum of shear wave of a sub-fault is described by sub-fault seismic moment, corner frequency, and distance from the observation point, as given in Eq. 1:

$$A(f) = \left\{ \frac{R^{\theta\varphi} FV/(4\pi\rho\beta^3) M (2\pi f)^2}{[1+f^2]} \right\} \left\{ \frac{\exp(-\pi f K) \exp\left(\frac{-\pi f R}{Q\beta}\right)}{R} \right\} \quad (1)$$

where M, f and R are the sub-fault seismic moment, corner frequency, and distance from the observation point, respectively. $R^{\theta\varphi}$ is radiation patte rn, F is free surface amplification, V is partition onto two horizontal components, ρ is density, β is shear wave velocity. A high-cut filter to model near surface kappa effects that caused to observe rapid spectral decay at high frequencies. Geometric attenuation is applicable for body-wave spreading in a whole space.

In this dynamic corner frequency model, the corner frequency is a function of time, and the rupture history controls the frequency content of the simulated time series of each sub-fault. The rupture begins with a high corner frequency and progresses to lower corner frequencies as the ruptured area grows up. Limiting the number of active sub-faults in the calculation of dynamic corner frequency can control the amplitude of lower frequencies (Motazedian, and Atkinson, 2005). Independency of radiation of high-frequency energy from sub-fault size and applicability of the method for a broader magnitude range are the advantages of the method.

For the validation of parameters, observed data can be used. There exist four strong ground motion recordings during the main shock of 2010 Haiti earthquake at the stations, namely GRTK, GTBY, MTDJ and SDDR, installed by Caribbean Network (CU-USGS). The whole ground motion waveforms only recorded at the SDDR station, which is the closest station with an epicentral distance of 131.6 km, are compared with the simulated data. The parameters of SDDR station are summarized in Table 2.

Table 2. Parameters of SDDR station and peak ground acceleration values (PGA) of observed horizontal components (USGS)

Lat/ Lon	Elevation (m)	Azimuth (°)	Epicentral distance (km)	PGA* (%g) EW	NS	Soil Class
18.9817°N/ 71.2880°W	589	66	131.6	1.03	1.15	Rock

Source Models

The fault rupture process of the 2010 Haiti earthquake and inferred spatial and temporal slip distributions on the causative fault plane have been studied by several researchers. In the present study, five source models are considered for the computation of ground motion as input to fragility analyses: Model-1 (Ozel et al., 2011), Model-2 (Hayes et al., 2010), Model-3 (Hashimoto et al., 2011), Model-4 (Sladen, 2013), and Model-5 (random source model).

Model-1:

The study by Ozel et al. (2011) considers a 60 km to 25 km fault model retrieved by the Kikuchi and Kanamori finite source inversion technique that uses broadband teleseismic body wave records. The derived rupture model points out unilateral rupture propagation commenced at the eastern side of the fault plane where the major seismic moment release occurred. The rupture front propagated westward and terminated at a site where the largest aftershocks occurred. A seismic moment of M_o=8.17 x 10^{19} Nm released on a 60 km-long fault plane. We divide the fault plane into 10 by 5 sub-faults along the strike and dip, respectively.

Model-2:

A 48 km to 21 km fault model is adjusted to account for the likely westward propagation of rupture seen in preliminary InSar results and body-wave directivity by Hayes et al. (2010). GSN broadband waveforms downloaded from the NEIC waveform server are used. 12 teleseismic broadband P waveforms, 8 broadband SH waveforms are analyzed, and 25 long period surface waves selected based upon data quality and azimuthal distribution.

Model-3:

Hashimoto et al. (2011) fit the satellite surface deformation data to a fault model (80x40 km) to determine fault structure, It is shown that slip occurred on a fault dipping northward at 42^o with large thrust components. The maximum displacement on the fault was about 4m at 10–20 km depth, offshore from the Tiburon peninsula. It is confirmed that the earthquake ruptured a blind thrust fault.

Model-4:

Sladen (2013) used 21 teleseismic P waveforms and 16 teleseismic SH GSN broadband waveforms to constrain the slip history based on a finite fault inverse algorithm. In the modeling, Sladen 2010 used a fault strike (262°) and dip angle (70°) taken from the GCMT which yield 4 m maximum displacement on a finite source with fault length of 35 km along strike and 25 km along dip.

Model-5

Random source model based on common fault parameters is used to determine the ground motion input for a simple rupture model. The parameters are chosen according to the compatibility of estimated data with observed data (SDDR).

Model Parameters

To define the source mechanism of the earthquake, finite fault technique requires the specification of the fault geometry including the dip and strike angles, depth of the fault, hypocenter location, and sub-fault size. Source parameters including the fault dimensions, the hypocenter, moment magnitude, sub-fault size, and slip distribution are taken from the fault models were described in the previous section.

The path effects are modeled through geometrical spreading, anelastic attenuation, and ground motion duration effects. Several models are tried for the path effects. Any empirical analysis to assume the parameters related to the path effects have not been done due to the lack of observed data. For the geometric attenuation model, 1/R model, which makes the residuals between the observed and simulated data less, is used. The fault orientation parameters are taken from the outcomes of inversion analysis. The site type of the stations is assumed as rock. (http://ears.iris.washington.edu/stationList.html?netCode=CU&gaussian=2.5).

We validate the model through comparison of the simulated waveforms and Fourier spectra with the observed data recorded by SDDR station within the frequency range of interest (0.6–25 Hz). We tested our model parameters through comparisons of simulated and observed acceleration Fourier spectra. We initially tried different stress-drop values to model the high-frequency spectral amplitudes and then fine-tuned the pulsing percentage value to adjust the lower frequency amplitudes.

Figure 1 compares the synthetic waveforms, Fourier amplitude and response spectra with the recorded data at SDDR station. We observe that the individual synthetic PGA values generally match well with the observations. The duration of the ground motions is well reproduced. For the sake of brevity, we only show the comparisons related to Model-1.

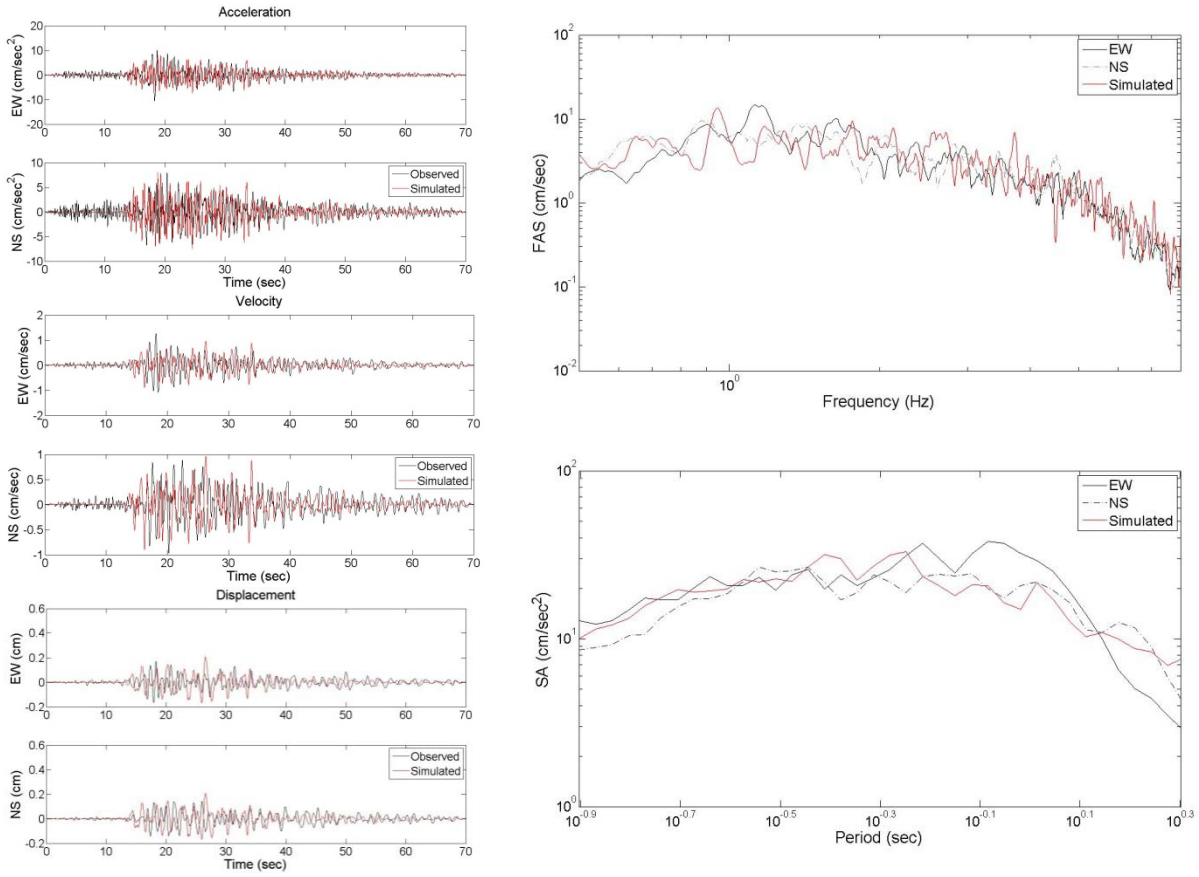

Figure 1. Comparison of simulated data based on Model 1 and observed data at SDDR station. The left column shows the acceleration (top), velocity (middle) and displacement (bottom) waveforms. The right column represents the Fourier amplitude spectrum (top) and response spectrum (bottom).

Site properties for each simulation point are taken from Cox et al. (2011) and Frankel et al. (2011) based on Wald and Allen (2007). Cox et al. presented a seismic site classification microzonation for the city of Port-au-Prince. The microzonation is based on 35 shear wave velocity (V_s) profiles collected throughout the city and a new geologic map of the region. The V_s profiles were obtained using the multichannel analysis of surface waves (MASW) method, while the geologic map was developed from a combination of field mapping and geomorphic interpretation of a digital elevation model (DEM). Much of the city is founded on deposits that classify as either NEHRP Site Class C or D, based onV_{S30} values.

Frankel et al. used the topographic slope on the basis of the methodology of Wald and Allen which provides an empirical relationship betweenV_{S30} and topographic slope to estimate the V_{S30} on a 1 km by 1 km grid across the Hispaniola. Areas of low estimated V_{S30} (<360 m/s, stiff or soft soils) in Haiti include portions of the Enriquillo Valley where Port-au-Prince is located and the delta of the Artibonite River.

Input Ground Motions for Fragility Analyses

PGA values at the locations of buildings are computed on the basis of stochastic finite-fault simulation methodology for five different source models and the selected model parameters as described in the previous sections. Ground motion simulations were conducted at 6,347 points for the locations of surveyed buildings in the field. In Figure 2, two examples illustrating the spatial distribution of PGA values for the geographic extend of the building locations in the field data set are presented. The ranges of PGA values, that the buildings in the field data set were experienced, with respect to previously defined data classes are given in Table 3.

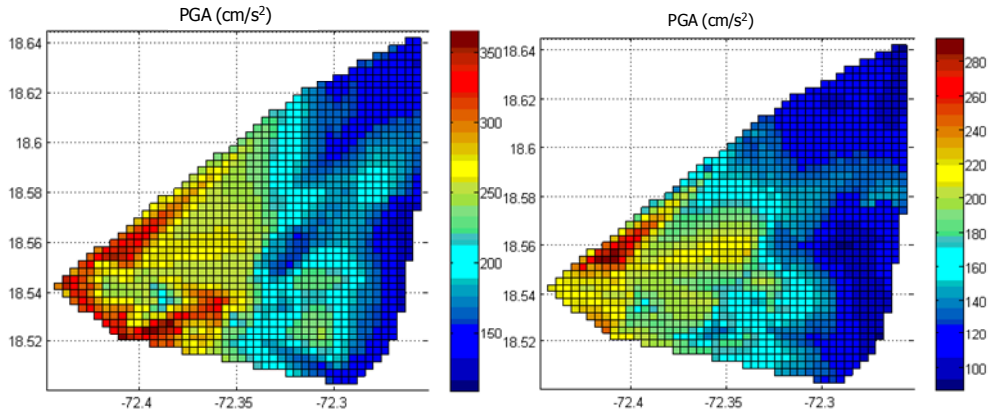

Figure 2. Spatial distribution of the simulated PGA values over the geographic extend of the building locations in the field data set: Model-2 (left) and Model-5 (right)

Table 3. Range of PGA values (in g) that the buildings in the field data set experienced.

	1-2 storey RC frame	3-5 storey RC frame	1-2 storey wooden frame
Model-1	0.10 - 0.43	0.12 - 0.37	0.12 - 0.38
Model-2	0.11 - 0.37	0.14 - 0.36	0.12 - 0.36
Model-3	0.07 - 0.27	0.09 - 0.24	0.09 - 0.27
Model-4	0.11 - 0.35	0.13 - 0.34	0.09 - 0.27
Model-5	0.06 - 0.23	0.06 - 0.22	0.06 - 0.22
Hancilar et al.	0.20 - 0.40	0.20 - 0.40	0.20 - 0.40

USGS SHAKE MAPS

Shortly after the event, the USGS published shaking intensity maps produced by ShakeMap software (v3.2) (Wald et al. 2005). ShakeMap generates maps of the spatial distribution of recorded peak ground motion parameters (acceleration, velocity, and spectral response) and of instrumentally derived seismic intensities [18]. Given the epicenter and magnitude of an earthquake (and for larger earthquakes, fault geometry if available), ShakeMap combines observed macroseismic intensities (including the USGS-Did You Feel It? System) with region-specific empirical ground motion estimations that utilize earthquake source and local geology information. For regions where there are insufficient strong ground motion recording stations (such as Haiti) to generate an adequate, strong-motion data-controlled ShakeMap, the software initially approximates a point source (hypocenter and magnitude) to constrain region-specific empirical ground motion estimations. Site amplification is then applied on the basis of relationships developed between topographic gradient and shear-wave velocity by [16]. When intensity data are used directly, the peak ground motion parameters are inferred from the macroseismic observations using empirical predictive equations.

In the previous study (Hancilar et al., 2013), for the derivation of fragility the GIS data associated with PGA shake maps with contour polygons at intervals of 0.04g were used.

DERIVATION OF FRAGILITY FUNCTIONS

The analytical expression used in this study for the derivation of fragility functions is the same as of is based on the assumption that earthquake damage distribution can be represented by the cumulative standard lognormal distribution function (Kircher et al., 1997). The conditional probability of damage being in or exceeding a particular damage state (DG_k) for a given level of ground motion intensity is given by the following relationship:

$$P\left[Damage \geq DG_k \left| IM \right. \right] = \Phi\left[(1/\beta) \ln(IM / \overline{IM}) \right] \quad (2)$$

where Φ is the standard normal cumulative distribution function, $\overline{IM}$ is the median value of the ground motion intensity measure (IM) for a given damage state (DG_k), and β is the log-standard deviation of the fragility curve.

For the estimation of two parameters of the fragility functions, i.e. median and standard deviation, maximum likelihood optimization is performed. In this process, proportions of the buildings (observations) being in or exceeding a given damage grade over the ground motion intensity range are obtained by the help of a Boolean vector. This is done by assigning a value of '1' to buildings experiencing damage equal to or greater than the specified damage grade and, a value of '0' to buildings with lesser damage than the specified damage grade. The numerical optimization is then performed and the two parameters of the fragility curve corresponding to the considered level of damage are obtained. For more information on the methodology, the reader is referred to Hancilar et al. (2013).

Fragility functions corresponding to five damage grades (i.e. DG-1 to 5) derived for 1-2 storey and 3-5 storey reinforced concrete buildings and for 1-2 storey wooden frame buildings on the basis of five different ground motion inputs are plotted in Figure 3. The previously constructed fragility curves are also shown on the same plots.

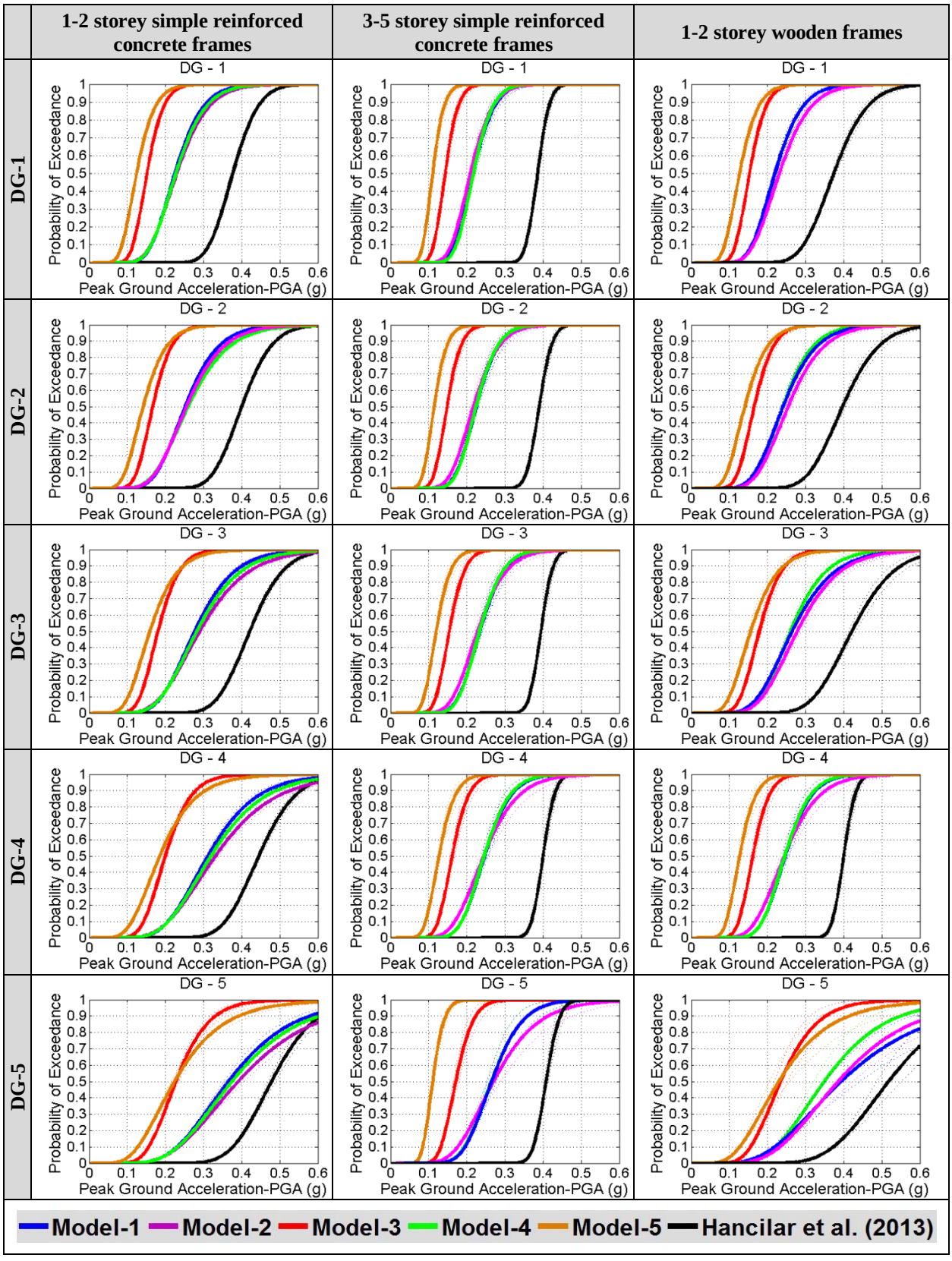

Figure 3. Comparison of fragility curves derived using different ground motion inputs

CONCLUSIONS

A great variability in the resulting fragility curves is observed in Figure 3. For a given level of ground motion intensity, the differences in the exceedance probabilities can be up to 70%. It is seen that for damage grades DG-1, -2 and -3, fragility functions resulting from Model-1, -2 and -4 are in good agreement. This might be mainly because of similar PGA ranges obtained from those three models. In general, the fragility functions of this study are very different than the previously developed fragility functions. The main reason for this might be the different ground motion intensity determinations. The ground motion input for the previously constructed fragilities is USGS shake maps, wherein PGA values are represented as isoseismic contours of 0.04g-intervals. In this case, all the buildings falling into the same contour experience the level ground motion intensity. In the present study, PGA value at each building location is computed by the ground motion simulation.

The results can be considered as evident of epistemic uncertainties arising from determination of ground motion intensity levels and their significant impacts on the computed fragility functions. The results show that changing the ground motion input in the derivation of empirical fragility functions causes significant variability in the resulting fragility functions

REFERENCES

Colombi M, Borzi B, Crowley H, Onida M, Meroni F, Pinho R. Deriving vulnerability curves using Italian earthquake damage data. Bull Earthq Eng 2008; 6: 485-504. doi: 10.1007/s10518-008-9073-6.

Corbane C, Carrion D, Lemoine G, Broglia M. Comparison of damage assessment maps derived from very high spatial resolution satellite and airborne imagery produced for the Haiti 2010 earthquake. *Earthquake Spectra* 2011; 27(S1): 199-218.

Cox, B., Bachhuber, J., Rathje, E., Wood, C., Dulberg, R., Kottke, A., Green, R., and Olson, S., (2011). Shear wave velocity- and geology-based seismic microzonation of Port-au-Prince,Haiti, Earthquake Spectra, 27, No. S1, S67–S92.

Frankel A., HarmsenS., Mueller C., Calais E., and HaaseJ., (2011) Seismic Hazard Maps for Haiti. Earthquake Spectra: October 2011, Vol. 27, No. S1, pp. S23-S41.

Grünthal G (editor). European Macroseismic Scale 1998 (EMS-98). In: Cahiers du Centre Européen de Géodynamique et de Séismologie, v. 15, 1998, Luxembourg.

Hancilar, U., Taucer F. and Corbane, C., (2013). Empirical fragility functions based on remote sensing and field data after the January 12, 2010 Haiti earthquake, *Earthquake Spectra* 2013; 29(4):1275-1310.

Hashimoto M., Fukushima, Y. and Fukahata Y. (2011), Fan-delta uplift and mountain subsidence during the Haiti 2010 earthquake, Nat Geosci, 4, 255-259.

Hayes G, Briggs R, Sladen A, Fielding E, Prentice C, Hudnut K, Mann P, Taylor F, Crone A, Gold R (2010), Complex rupture during the 12 January 2010 Haiti earthquake. Nat Geosci 3:800–805.

Kircher CA, Nassar AA, Kustu O, Holmes WT. Development of building damage functions for earthquake loss estimation. Earthq. Spectra 1997; 13(4): 663-682. doi: 10.1193/1.1585974.

Motazedian, D., and Atkinson G. M. (2005). Stochastic finite-fault modelingbased on a dynamic corner frequency, Bull. Seismol.Soc. Am. 95,995–1010.

Ozel MN, Harmandar E. and Pınar A (2011). Sensitivity of the strong ground motion time histories to a finite source model: A case study for the January12, 2010 Haiti earthquake (Mw=7.0). Soil Dyn Earthquake Eng,doi:10.1016/j.soildyn.2011.06.004.

Rossetto T., Ioannou I., Grant D.N. Existing empirical fragility and vulnerability functions: Compendium and guide for selection, GEM Technical Report 2013-X, GEM Foundation, Pavia, Italy.

Rota M, Penna A, Strobbia CL. Processing Italian damage data to derive typological fragility curves. Soil Dyn Earthquake Eng 2008; 28: 933-947.

Sarabandi P, Pachakis D, King SA, Kiremidjian AS. Empirical fragility functions from recent earthquakes. In: Proceedings of the 13th World Conference on Earthquake Engineering, 2004 Vancouver, Canada.

ShakeMap 2011: ShakeMap Scientific Background, http://earthquake.usgs.gov/earthquakes/shakemap/background.php#wald99a.

Sladen A. (Caltech, Haiti 2010). Preliminary Result 01/12/2010 (Mw 7.0), Haiti. Source Models of Large Earthquakes. http://www.tectonics.caltech.edu/slip_history/2010_haiti/index.html, last accessed July 1, 2013.

Spence R.J.S., Coburn A.W., Pomonis A., (1992). Correlation of ground motion with building damage: The definition of a new damage-based seismic intensity scale, Proceedings of 10th World Conference on Earthquake Engineering, Balkema, Rotterdam.

Wald DJ, Worden BC, Quitoriano V, Pankow KL. ShakeMap manual: technical manual, user's guide, and software guide. U.S. Geological Survey Techniques and Methods 2005, Book 12, Section A, Chap. 1. Reston, Virginia, U.S. Geological Survey: 132.

Wald, D. J., and Allen, T.I., (2007). Topographic slope as a proxy for seismic site conditions andamplification, Bull. Seism. Soc. of Am. 97, 1379–1395.